Desalination and Water Treatment
www.deswater.com

doi:10.5004/dwt.2019.23831

148 (2019) 338–350
April

Solar light assisted degradation of oxytetracycline from water using Bi_2O_3/Fe_3O_4 supported graphitic carbon nitride photocatalyst

Pankaj Raizada[a,*], Anita Sudhaik[a], Virender Pratap Singh[b], Vinod Kumar Gupta[c], Ahmad Hosseini-Bandegharaei[d,e], Rajesh Kumar[b], Pardeep Singh[a]

[a]*School of Chemistry, Faculty of Basic Sciences, Shoolini University, Solan (HP)-173229, India, email: pankajchem1@gmail.com (P. Raizada), sudhaikanita@gmail.com (A. Sudhaik), pardeepchem@gmail.com (P. Singh)*
[b]*School of Physics, Faculty of Basic Sciences, Shoolini University, Solan (HP)-173229, India, email: kunwar.virender@gmail.com (V.P. Singh), rajesh.shoolini@gmail.com (R. Kumar)*
[c]*Department of Biological Sciences, Faculty of Science, King Abdulaziz University, Jeddah, Saudi Arabia, email: vinodfcy@gmail.com (V.K. Gupta)*
[d]*Wastewater Division, Faculty of Health, Sabzevar University of Medical Sciences, PO Box 319, Sabzevar, Iran*
[e]*Department of Engineering, Kashmar Branch, Islamic Azad University, PO Box 161, Kashmar, Iran, email: ahoseinib@yahoo.com (A. Hosseini-Bandegharaei)*

Received 5 September 2018; Accepted 21 January 2019

ABSTRACT

The undesirable release of antibiotics into natural water bodies is regarded as major threat to aquatic environment. The fabrication of magnetically separable photocatalyst with high stability and recycle efficiency is emerging as an important strategy to mitigate water pollution. This research work reports a facile fabrication of ternary nanocomposite comprising of g-carbon nitride (GCN) and Bi_2O_3/Fe_3O_4. GCN was synthesized via calcination method involving thermal condensation of melamine. FESEM, HRTEM, FTIR, EDX, XRD, PL and UV-visible spectroscopy verified the successful preparation of GCN/Bi_2O_3/Fe_3O_4. The as synthesized GCN/Bi_2O_3/Fe_3O_4 photocatalyst was tested for the photocatalytic degradation and mineralization of oxytetracycline (OTC) antibiotic as target pollutant under solar light irradiation. GCN/Bi_2O_3/Fe_3O_4 revealed excellent photocatalytic performance for the degradation of OTC as compared to GCN and Bi_2O_3 due to suitable band gap positions. The synergistic adsorption and photocatalysis exhibited significantly higher efficacy for OTC degradation. The OTC was fully mineralized in 8 h in visible light exposure. GCN/Bi_2O_3/Fe_3O_4 was recovered from reaction mixture in 90 s employing a magnet and recycled for 10 consecutive cycles without much loss in catalytic activity. The present study attempts to provide a new approach for the designing of an efficient magnetic photocatalyst for organic pollutant eradication from simulated water.

Keywords: Graphitic carbon nitride; Bi_2O_3/Fe_3O_4; Photocatalysis; Antibiotic degradation; Fast separation

1. Introduction

Oxytetracycline (OTC) pertains to a class of pharmaceuticals and used worldwide as well as enters into aquatic environment polluting water system due to their toxicity after discharge into several water sources [1,2]. Antibiotics are toxic to ecosystem; enter via sewage release from pharmaceutical industries, hospitals and domestic waste. Nowadays, rise in antibiotic resistant bacteria growth is generating a major problem in wastewater purification [3,4]. Oxytetracycline (OTC) antibiotic is repeatedly identified tetracycline in aquatic system that is entering as a pollutant in water resources [5]. Numerous traditional methods of wastewater purification were employed including filtration, coagulation,

*Corresponding author.

sedimentation, adsorption and reverse osmosis. Above mentioned conventional methods proved inefficient for purification of polluted water from pesticides, pharmaceutical, organic solvents and household chemicals [6].

Advanced oxidation processes (AOPs) emerged as a proficient technique for the removal of biotic/abiotic pollutants from wastewaters. Among AOPs, semiconductor-based photocatalysis has received a great attention in recent years [7]. The development of a visible light assisted photocatalyst is critically desired for the utilization of solar light. The coupled metal oxide semiconductors emerged proficient photocatalytic materials for environmental wastewater treatment via mineralization of biotic/abiotic pollutants under visible and UV light irradiation [8]. Graphitic carbon nitride (GCN) is a promising metal-free photocatalytic material endowed with excellent photocatalytic properties for water purification under visible-light irradiation [9]. Carbon nitride (GCN) is non-toxic, chemically and thermally stable, π-conjugated compound exhibiting versatile optical and electronic properties with a suitable band gap [10–14]. Apart from its good properties, material is also inherited with its limitations including electron-hole pair recombination and restricted visible light exploitation for water purification [15].

Bismuth trioxide (Bi_2O_3) is regarded as a potential photocatalyst due to its lower band gap energy (2.8 eV) with beneficial electrical properties, remarkable photoconductivity and good photoluminescence [16,17]. Bismuth oxide (Bi_2O_3) is characterized with various advantages such as catalysis, ceramics, solid-state electrolytes and chemical sensors owing to its more surface area assisting in increased adsorption sites. But on the contrary suffers from some drawbacks as high corrosion activity and low mechanical strength [18,19]. Bi_2O_3 based nanocomposites were previously reported to be an efficient photocatalyst for industrial wastewater remediation containing OTC antibiotics as pollutants [20]. Apart from all these, magnetic separation of the photocatalyst is of great interest due to its logical and technical relevance in wastewater treatment [21–23]. Many magnetic spinel structured ferrite nanoparticles have been employed for proficient separation of nanoparticles from treated water [24–26]. The introduction of Fe_3O_4 led to rapid separation and recovery of photocatalyst *via* magnet [27–30]. The heterojunction engineering with desired electronic properties was performed for overcoming the aforementioned drawbacks of conventional photocatalyst for the successful separation of charge carriers [31,32].

Oxytetracycline antibiotic was selected as target pollutant for the exploration of photodegradation. This piece of research work reports the facile synthesis of magnetically separable ternary GCN/Bi_2O_3/Fe_3O_4 photocatalyst. The as synthesized GCN/Bi_2O_3/Fe_3O_4 photocatalyst was characterized using various physical and chemical techniques including Fourier emission scanning electronmicroscope (FESEM), transmission electron microscopy (HRTEM), X-ray diffraction (XRD), Fourier-transform infrared spectroscopy (FTIR) and energy-dispersive, X-ray spectroscopy (EDX) analysis, UV-visible analysis and BET. The cooperative influence of adsorption and photocatalysis on OTC degradation was investigated. Lastly, detailed mechanism of OTC mineralization was also explored under solar light irradiation.

2. Experimental

2.1. Preparation of GCN/Bi_2O_3/Fe_3O_4

Bismuth nitrate pentahydrate [$Bi(NO_3)_3{\cdot}5H_2O$], citric acid [$C_6H_8O_7{\cdot}H_2O$], $FeCl_3{\cdot}6H_2O$, $FeCl_2{\cdot}4H_2O$, NH_4OH, HNO_3 (0.04 mol/L) were purchased from Ranbaxy (India) PEG-4000, Melamine were purchased from Sigma Aldrich, India. All aqueous solutions were prepared in deionized water.

2.1.1. Fabrication of GCN

In brief, GCN was synthesized via thermal polycondensation of melamine at 450–650°C. Firstly, 5 g of melamine was calcined for 2 h at 450°C and then further heated up to 650°C with 10°C temperature rise per min. With the increase in temperature from 450°C to 650°C, yellow colored powder was attained. The resultant yellow powder was cooled and crushed into fine powder form using pestle and mortar and labelled as GCN for further use.

2.1.2. Synthesis of GCN/Bi_2O_3 binary composite

GCN/Bi_2O_3 binary nanocomposite was synthesized *via* modified hydrothermal method. Typically, 1 g GCN was dispersed in 100 ml of H_2O and sonicated for 20 min. Then, 2.9 g of $Bi(NO_3)_3{\cdot}5H_2O$ and 1.4 g of citric acid were dissolved separately in deionized H_2O:HNO_3 solution (0.04 mol) having 90 ml : 10 ml ratio. The obtained reaction mixture was added to GCN suspension. The resultant solution was then heated at 300°C for 2 h to obtain GCN/Bi_2O_3 powder (Fig. 1). Bi_2O_3 nanoparticles were prepared by adopting exactly same methodology but deprived of GCN.

2.1.3. Synthesis of GCN/Bi_2O_3/Fe_3O_4 ternary nanocomposite

GCN/Bi_2O_3/Fe_3O_4 was prepared employing an *in-situ* precipitation method. Typically, 1 g of GCN/Bi_2O_3 powder was dispersed in 100 ml deionised water and magnetically stirred for 15 min followed by ultrasonication for next 20 min in a beaker. In another beaker, 1.8 g of $FeCl_3{\cdot}6H_2O$ and 0.8 g of $FeCl_2{\cdot}4H_2O$ were dissolved in 40 ml distilled water and continuously stirred on a magnetic stirrer for 20 min. Then both the above solutions taken in both beakers were mixed and obtained final solution was magnetically stirred at 80°C for 20 min. To this reaction mixture, 20 ml of NH_4OH was quickly injected. The resulting mixture was sonicated for 10 min followed by cooling and several times washing with water and finally with ethanol. Lastly, as obtained precipitates of GCN/Bi_2O_3/Fe_3O_4 were oven dried at 70°C and preserved for experimental studies (Fig. 1). Fe_3O_4 nanoparticles were prepared employing same methodology with no addition of GCN/Bi_2O_3 to reaction solution.

2.2. Photocatalytic activity experiment

Photocatalytic efficiency of synthesized GCN/Bi_2O_3/Fe_3O_4 nanocomposite was investigated for OTC degradation in 250 ml double walled beaker (borosilicate) using thermostatic water movement arrangement (25±0.3°C). Briefly, 0.50 g of powdered photocatalyst was added to 50 mL aqueous solution of OTC. Digital lux-meter ($35 \times 10^3 \pm 1000$lx) was used to measure solar light intensity. The solution contain-

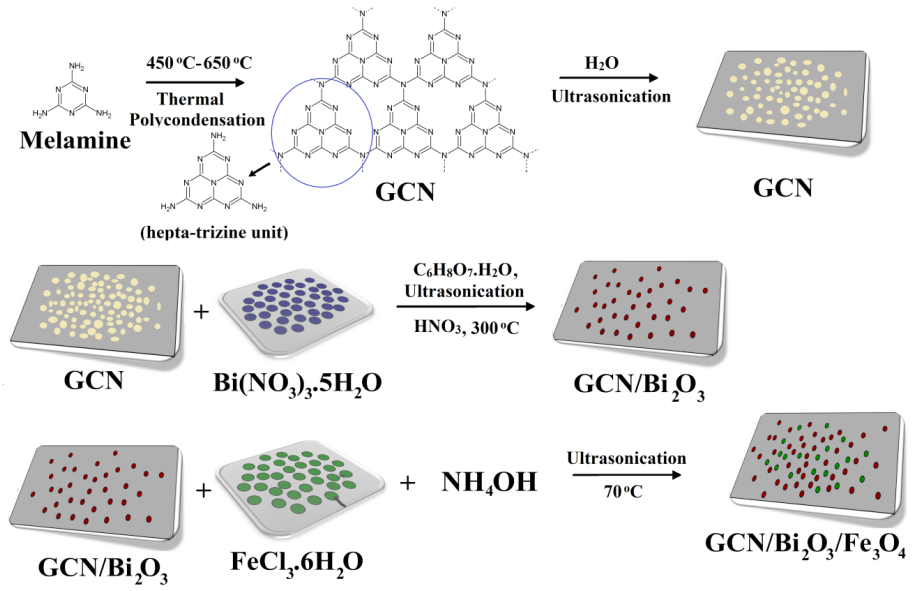

Fig. 1. Schematic preparation of GCN/Bi_2O_3/Fe_3O_4 photocatalyst.

ing OTC and photocatalyst was continuously stirred to avoid agglomeration of catalyst. 2 mL aliquot was withdrawn and separation of photocatalyst particles from aliquot was performed *via* a magnet. The resulting clear aliquot was analyzed on UV–Vis spectrophotometer to record the change in oxytetracycline concentration. Photocatalytic experiments were accomplished between April to June 2017 (10 am to 2 pm) month. Chemical oxygen demand (COD) was estimated through closed reflux technique. For the determination of unreacted oxidant, samples were titrated with Mohr's salt and ferroin indicator. COD and CO_2 amounts were also accomplished *via* earlier reported approaches and removal efficiency has been calculated using Eq. (1).

$$\%\ removal\ efficiency = \frac{C_0 - C_t}{C_0} \tag{1}$$

where C_0 signifies initial concentration and C_t/COD indicated instant concentration of sample/COD. Eqs. (2) and (3) were used for the calculation of rate constant (k) and half-life period ($t_{1/2}$):

$$k = 2.303 \times slope \tag{2}$$

$$t_{\frac{1}{2}} = \frac{0.693}{k} \tag{3}$$

Slope was achieved from plot of ln (c) vs. 't'.

3. Results and discussion

3.1. Morphological and structural characterization of GCN/Bi_2O_3/Fe_3O_4

3.1.1. FESEM, TEM, HRTEM and XRD analysis of GCN/Bi_2O_3/Fe_3O_4

FESEM images for GCN, GCN/Bi_2O_3 and GCN/Bi_2O_3/Fe_3O_4 are shown in Figs. 2a–f. Graphitic carbon nitride exhibited graphite-like layered structure with rough, irregular and porous surface shown in Figs. 2a and b. The uneven porous surface facilitated OTC adsorption on its surface. The deposition of $Bi_2O_3$and Fe_3O_4 on GCN surface is clearly seen in Figs. 2c–f. The formation of GCN/Bi_2O_3/Fe_3O_4 nanocomposite was further analyzed by TEM and HRTEM analysis. High-resolution transmission electron microscopy (HRTEM) permits direct imaging of sample at atomic level. GCN exhibited sheet like structure with lattice fringe of 0.16 nm (Figs. 3a and b). In Figs. 3c–f, the dispersion of both Bi_2O_3 and Fe_3O_4 onto GCN was observed. The clear lattice fringes were observed and separated by distance 0.16 nm (GCN), 0.339 nm (Bi_2O_3), 0.334 nm (Bi_2O_3 in GCN/Bi_2O_3), 0.14 nm (GCN in GCN/Bi_2O_3) and 0.202 nm [33,34].

The crystal structure of as-prepared GCN/Bi_2O_3/Fe_3O_4 ternary photocatalyst was examined by powdered XRD analysis (Fig. 4). In XRD spectrum of GCN, diffraction peaks at 13.1° and 27.4° corresponded to (100) and (002) plane, respectively [35,36]. The peak at 13.1° was ascribed to in-plane structural packing motif of tri-s-triazine units and other dominant peak at 27.4° was corresponded to inter-planer stacking reflection of aromatic sections of GCN tetragonal phase (JCPDS 87-1526) [37]. Fig. 4 shows XRD pattern as synthesized Bi_2O_3 sample. The characteristic peaks at position of 28.02°, 32.3°and 46.2°corresponded to (201), (200) and (222) planes respectively and specified monoclinic structure of Bi_2O_3(JCPDS65-1209) [38,39]. In XRD spectrum of GCN/Bi_2O_3/Fe_3O_4 nanocomposite, diffraction peaks at 2θ = 30.4°, 35.7°, 43.4°, 53.4° and 57.4° were attributed to (220), (311), (400), (422), (511) planes of Fe_3O_4. The characteristic peaks of both GCN and Bi_2O_3 at 13.1°, 27.4°, 32.3° and 46.2° were assigned to (100), (002), (200) and (222) planes, respectively in GCN/Bi_2O_3/Fe_3O_4. Bonding between GCN, Bi_2O_3 and Fe_3O_4 lead to improvement in intensity. XRD pattern also confirmed the semi-crystalline structure of nanocomposite. From above discussion, it was inferred that Fe_3O_4 were successfully deposited on the sur-

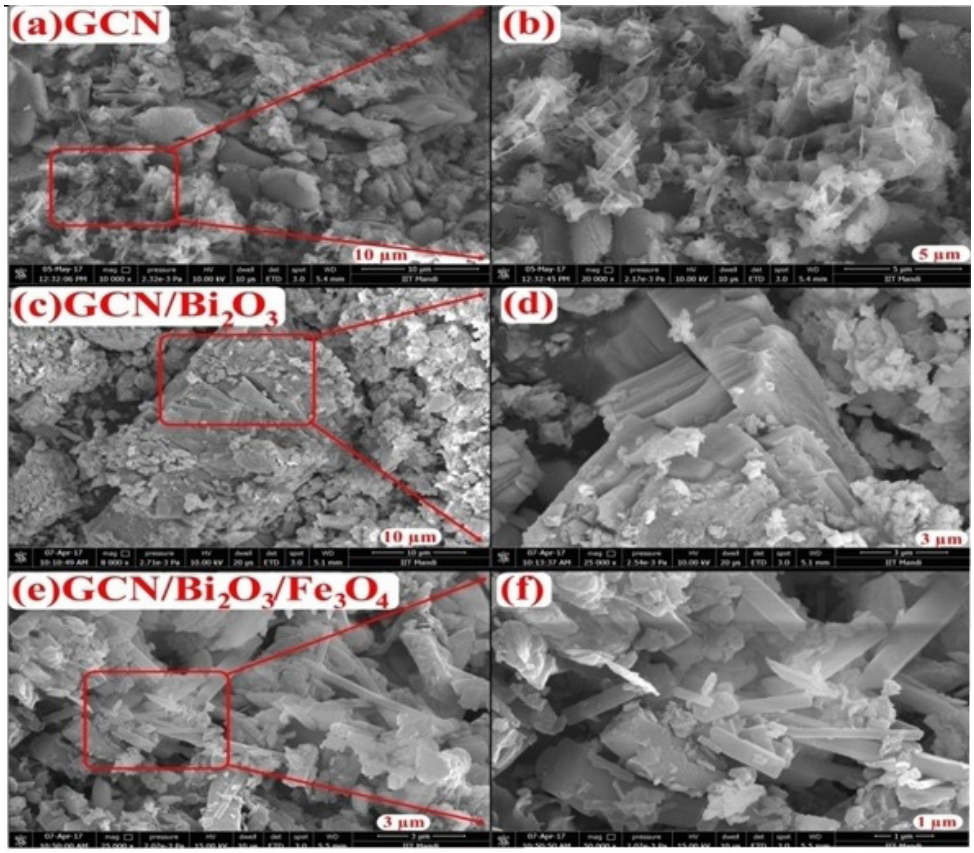

Fig. 2. SEM & FE-SEM images of GCN (a and b), GCN/Bi_2O_3 (c and d) and GCN/Bi_2O_3/Fe_3O_4(e and f).

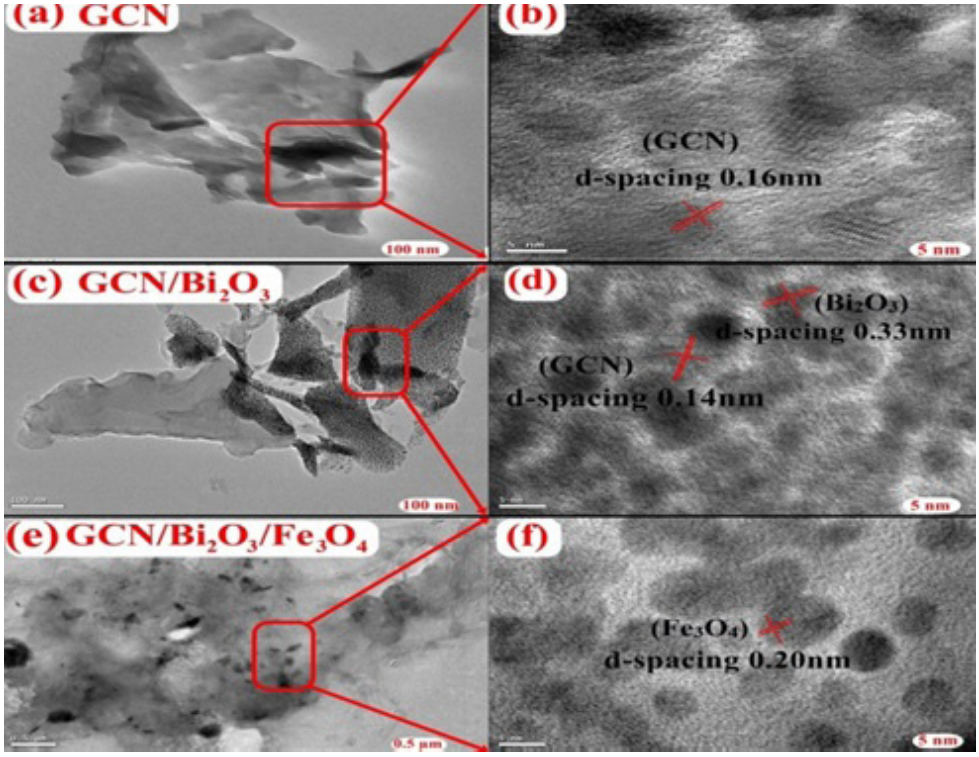

Fig. 3. HRTEM images of GCN(a-b), GCN/Bi_2O_3(c-d) and GCN/Bi_2O_3/Fe_3O_4 ternary composite (e-f).

face of GCN sheet along with Bi_2O_3 by in situ growth mechanism. No free Fe_3O_4 or Bi_2O_3 nanoparticles were found outside GCN sheet that also prevented the agglomeration of both Bi_2O_3 and Fe_3O_4 nanoparticles [40].

3. 1.2. FTIR and EDX, BET analysis of GCN/Bi_2O_3/Fe_3O_4

Fig. S1 shows FTIR spectra of GCN, Bi_2O_3, GCN/Bi_2O_3 and GCN/Bi_2O_3/Fe_3O_4 composites. The aromatic C-N stretching was observed in the region of 1252–1640 cm^{-1} (1241, 1319, 1411, 1457, 1569, 1639 cm^{-1}). The band owing to out of plane bending mode of tri-s-triazine units (heptazine rings) was recorded at 811 cm^{-1} [41]. A group of broad peaks was obtained from 3200-3400 cm^{-1} which corresponded to N-H bonds stretching vibration in primary amine (–NH_2). In Bi_2O_3, The cluster of peaks from 500–600 cm^{-1} was assigned to Bi-O stretching vibrations. The peaks at 862, 762 and 903 cm^{-1} were corresponded to stretching vibration of Bi-O-Bi [42]. The absorption band at 3450 cm^{-1} was assigned to O-H bending vibration. In spectrum of GCN/Bi_2O_3, characteristic peaks of both GCN and Bi_2O_3 were recorded. FTIR spectrum of GCN/Bi_2O_3/Fe_3O_4 displayed characteristic Fe-O peak at 583 cm^{-1}. The peaks of both GCN and Bi_2O_3 were also recorded in GCN/Bi_2O_3/Fe_3O_4. The slight shift in the intensity of peak indicated the formation of GCN/Bi_2O_3/Fe_3O_4.

EDX spectra of GCN, Bi_2O_3, GCN/Bi_2O_3 and GCN/Bi_2O_3/Fe_3O_4 are shown in Figs. 5a–d. EDX spectrum of GCN displayed an elemental composition of carbon (C) and nitrogen (N) elements (Fig. 5a) and Bi_2O_3 revealed the existence of bismuth (Bi) and oxygen (O) elements (Fig. 4b). In Fig. 5c, EDX spectrum of GCN/Bi_2O_3 confirmed the presence of bismuth (Bi), oxygen (O), carbon (C) and nitrogen (N) elements. EDX spectrum and percentage atomic composition of GCN/Bi_2O_3/Fe_3O_4 is shown in Fig. 5d. The occurrence of carbon (C), nitrogen (N), bismuth (Bi), oxygen (O) and Iron (Fe) elements indicated the formation of ternary GCN/Bi_2O_3/Fe_3O_4. Adsorption/desorption isotherm of N_2 in GCN/Bi_2O_3/Fe_3O_4 nanocomposite is presented in Figs. 6a, b and type IV isotherm with mesoporous nature was revealed by GCN in GCN/Bi_2O_3/Fe_3O_4 nanocomposite (specific surface area is 80.8 m^2/g and 72.0 m^2/g) [43,44].

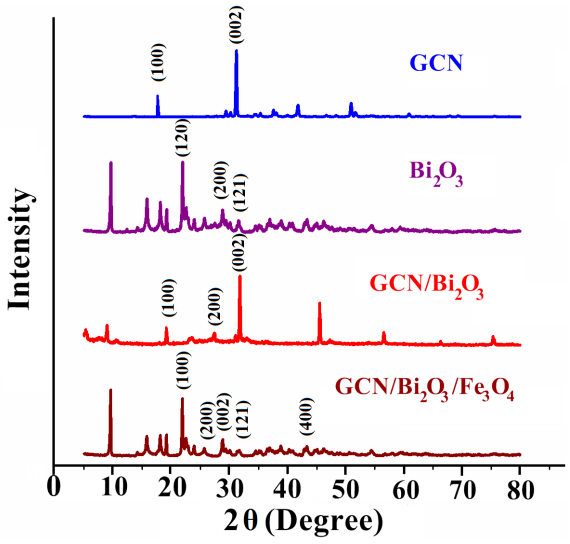

Fig. 4. XRD of spectra of GCN, Bi_2O_3, GCN/Bi_2O_3, GCN/Bi_2O_3/Fe_3O_4.

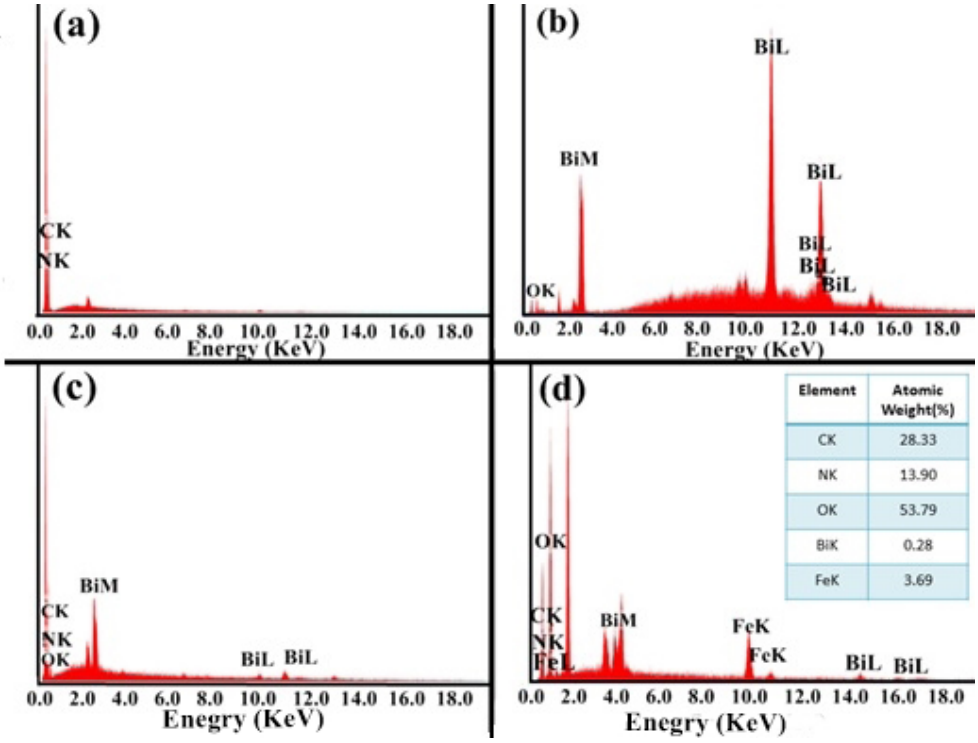

Fig.5. EDX spectra of GCN, Bi_2O_3,GCN/Bi_2O_3 binary composite and GCN/Bi_2O_3/Fe_3O_4.

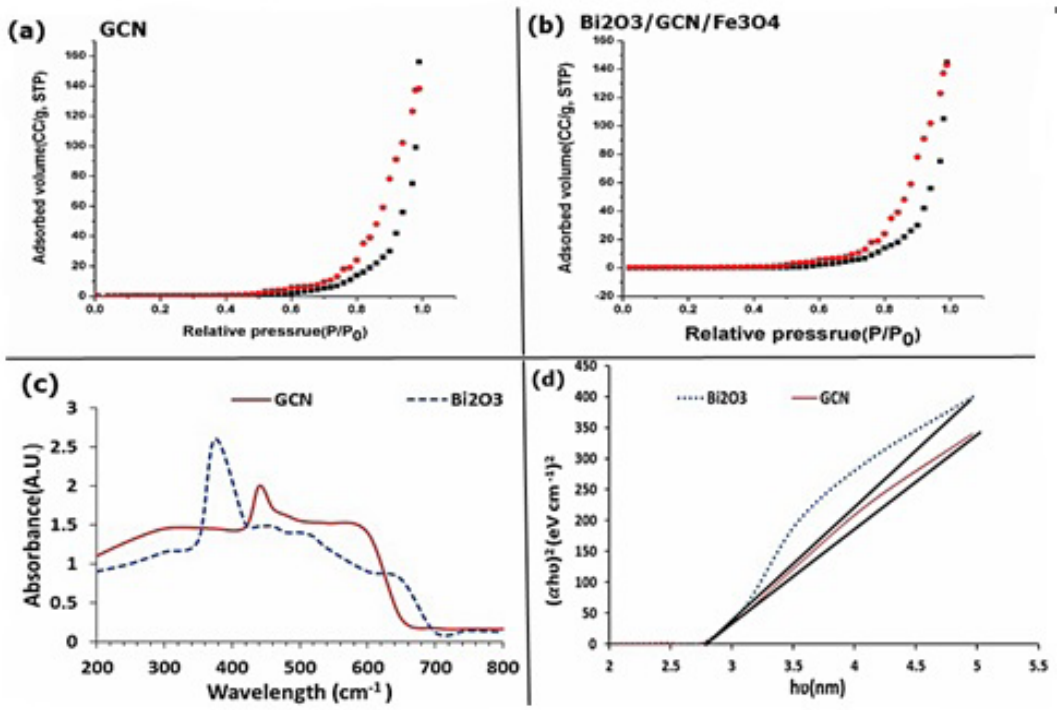

Fig. 6. (a) BET analysis of GCN, (b) BET analysis of GCN/Bi_2O_3/Fe_3O_4, (c) UV-visible analysis GCN and Bi_2O_3 and (d) Tauc's plot of GCN and Bi_2O_3.

3.1.3. UV-Visible, band gap analysis and magnetization study of GCN/Bi_2O_3/Fe_3O_4 nanocomposite

Fig. 6 (c and d) presented UV-visible spectra and Tauc's plots of GCN/Bi_2O_3/Fe_3O_4 nanocomposites. For the analysis of band gap, 2 mg/10 mL concentration of Bi_2O_3 and GCN was dispersed in ethanol (Figs. 6c and d) and absorption edges of Bi_2O_3 and GCN was obtained at 380 nm and 460 nm, respectively. Tauc's plot was applied for the calculation of optical band gap using the formula:

$$\alpha h\upsilon = B\left(h\upsilon - E_g\right)^n \quad (4)$$

where α denotes absorption coefficient = 2.303 A/l, E_g signifies optical band gap, B implies band tailing parameter, $h\upsilon$ indicates photon energy and n connotes ½ for direct band gap. Straight line curve was extrapolated between ($\alpha h\upsilon$)and $h\upsilon$ for the determination of optical band gap, when α = 0. The calculated band gap of GCN and Bi_2O_3 was 2.7 and 2.8 eV, respectively.

In slurry type photoreactors, recovery of photocatalyst is an important issue for its practical applications. The photocatalyst should be magnetic in nature for rapid separation from reaction solution. Magnetization study of Fe_3O_4 and GCN/Bi_2O_3/Fe_3O_4 nanocomposite is exposed in Figs. 7a and c due to applied magnetic field. Fe_3O_4 and GCN/Bi_2O_3/Fe_3O_4, both had respective saturation magnetization (M_s) of 16.82 and 14.34 emu/g. Existence of non-magnetic GCN/Bi_2O_3 in GCN/Bi_2O_3/Fe_3O_4 nanocomposite was confirmed by lower M_s values and intensity of applied magnetic field weakens to zero indicated by hysteresis loop (M-H curve) [45]. Magnetic remanance (M_r) of Fe_3O_4 and GCN/Bi_2O_3/Fe_3O_4 nanocomposite was perceived as 11.35 and 11.33 emu/g. On applying external magnetic field, easier separation of GCN/Bi_2O_3/Fe_3O_4 nanocomposite was observed from treated water. These magnetic studies marked superparamagnetic behavior of Fe_3O_4 and GCN/Bi_2O_3/Fe_3O_4 nanoparticles. GCN/Bi_2O_3/Fe_3O_4 and Fe_3O_4 nanoparticles can be easily separated from treated water in 90 and 60 s by employing a permanent magnet close to bottle after performing photocatalytic experiments (Figs. 7b and d).

3.2. Eradication of oxytetracycline antibiotic under various reaction conditions

Photocatalytic experiment was performed to measure photocatalytic activity of GCN, GCN/Bi_2O_3 and GCN/Bi_2O_3/Fe_3O_4 nanocomposite under solar light for Oxytetracycline antibiotics degradation (Fig. 8a). The photocatalytic efficiency of used photocatalysts followed the trend as: GCN/Bi_2O_3/Fe_3O_4 (94%) > GCN (65%) > Bi_2O_3 (58%) >> Fe_3O_4 (9%). The obtained trend revealed quite higher efficiency of GCN/Bi_2O_3/Fe_3O_4 as compared to as Bi_2O_3 and GCN, while Fe_3O_4 had minimal photocatalytic activity for OTC degradation. In case of surface assisted photo-degradation reactions, adsorption of aqueous phase pollutant is considered as an important factor for efficient catalytic removal of pollutants. The removal experiments were also conducted in dark to assess adsorbent nature of used photocatalyst (Fig. 8b). The adsorption ability of used adsorbents followed the trend: GCN/Bi_2O_3/Fe_3O_4 (52%) ≈ GCN (50%) > Bi_2O_3 (15%) > Fe_3O_4 (9%). In this work, GCN had emerged as an effective adsorbent for OTC removal. While both Bi_2O_3 and

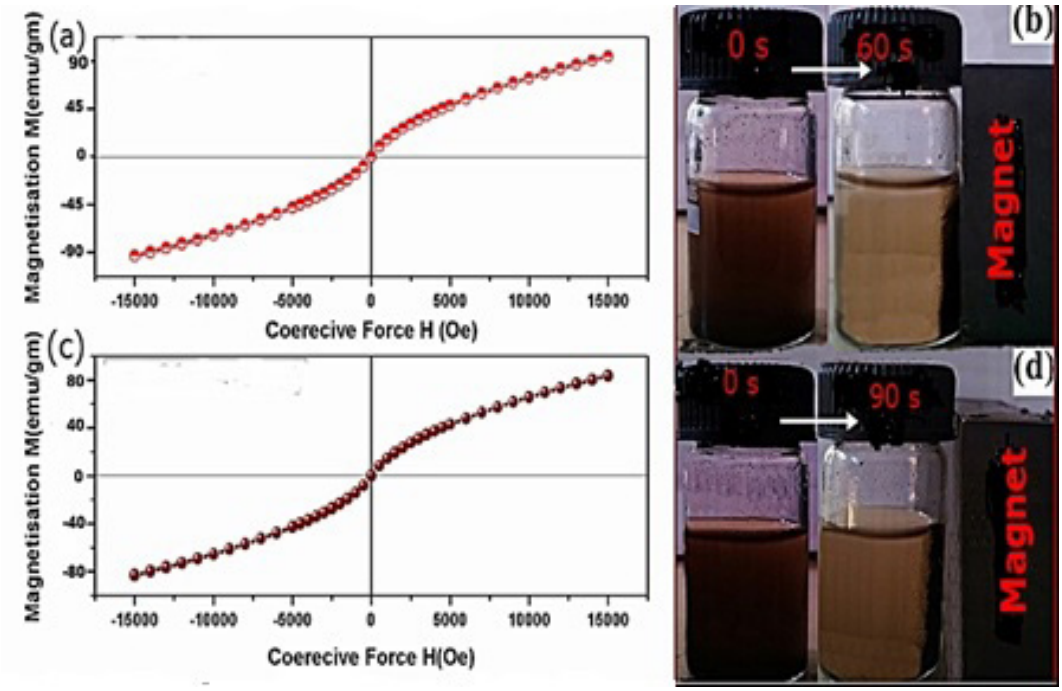

Fig. 7. (a) Hysteresis curve of Fe_3O_4, (b) Magnetic separation of Fe_3O_4, (c) Hysteresis curve of GCN/Bi_2O_3/Fe_3O_4 and (d) Magnetic separation of GCN/Bi_2O_3/Fe_3O_4.

Fe_3O_4 displayed quite low adsorption ability as compared GCN. Photodegradation of OTC antibiotic was affected by adsorption ability of as synthesized GCN. So furthermore, two different reaction conditions were employed for OTC photodegradation i.e. (i) Equilibrium adsorption proceeded after photodegradation (A-P) and (ii) concurrent adsorption with photocatalysis (A+P). GCN/Bi_2O_3/Fe_3O_4 nanocomposite performed 95% of OTCe radication in 60 min under solar light during A+P approach and only 60% of OTC was removed in case of A-P approach (Fig. 8c). Thus efficiency of investigated photocatalytic systems for OTC eradication followed trend: GCN/Bi_2O_3/Fe_3O_4/A+P>GCN//Bi_2O_3/Fe_3O_4/DA>GCN/Bi_2O_3/Fe_3O_4/A-P. From the results, it was also perceived that A+P system have higher OTC removal than A-P system. The efficiency trend of processes was observed as: A+P > DA > A-P. A-P possessed lowest removal due to retarding influence of adsorption on photocatalytic process [46,47]. The additional adsorbed pollutant (OTC antibiotic) behaved as a sieve for solar light and retarded the photo active volume that diminished pollutant degradation. Therefore, A+P process with adsorption and photocatalysis eliminated adsorbed OTC molecule through photodegradation process. Thus combination of (binary composite) GCN and Bi_2O_3 had a synergistic effect on OTCe radication due to coupling of adsorption and photocatalytic process [48].

3.3. Influence of different reaction parameters on OTC photodegradation using GCN/Bi_2O_3/Fe_3O_4/A+P catalytic system

For the optimization of different reaction parameters for OTC degradation, different reaction factors like OTC concentration, catalyst loading and pH were studied to evaluate photocatalytic performance of GCN/Bi_2O_3/Fe_3O_4/A+P system. The outcomes were interpreted in the form of half-life time ($t_{1/2}$) and first order rate constant (k). Variation in the initial concentration of oxytetracycline antibiotic was from 0.7×10^{-4} mol dm^{-3} to 9×10^{-4} mol dm^{-3} and increment in rate constant was observed from 3.5×10^{-4} s^{-1} to 5.5×10^{-4} s^{-1} with the proliferation in OTC concentration i.e. 7.0×10^{-4} mol dm^{-3} to 1.0×10^{-4} mol dm^{-3}. Thereafter, decrease in rate constant was perceived from 5.5×10^{-4} s^{-1} to 3.8×10^{-4} s^{-1} with the enhancement in OTC concentration from 1.0×10^{-4} mol dm^{-3} to 9.0×10^{-4} mol dm^{-3}. Rate constant was found maximal at 1.0×10^{-4} mol dm^{-3} concentration for OTC antibiotic due to occurrence of OTC molecules in photoactive volumes in photodegradation process. However, OTC represented itself as a sieve for incident irradiation and minimized photoactive volume [49]. Analysis of catalyst dose effect on OTC degradation was examined by increase in amount of GCN/Bi_2O_3/Fe_3O_4 nanocomposite (ternary composite) from 10 mg/50 mL to 120 mg/50 mL and it was confirmed that rate constant upgraded from 1.5×10^{-2} min^{-1} to 5.4×10^{-2} min^{-1} with the enhancement in loading of GCN/Bi_2O_3/Fe_3O_4 nanocomposite. It was also scrutinized that rate constant of photocatalyst loading was utmost at 60 mg/50 mL. Increase in catalyst loading also leaded to enhancement inactive site numbers for photodegradation of OTC molecule. However, increased catalyst loading also resulted in formation of turbid solution which retarded reaction rate by blocking the sunlight penetration in photoactive volume. It can be anticipated that for effective photodegradation of OTC, ideal amount of GCN/Bi_2O_3/Fe_3O_4 nanocomposite was required so that obtain ability of light photons can be confirmed and extra photocatalyst can be avoided [50,51].

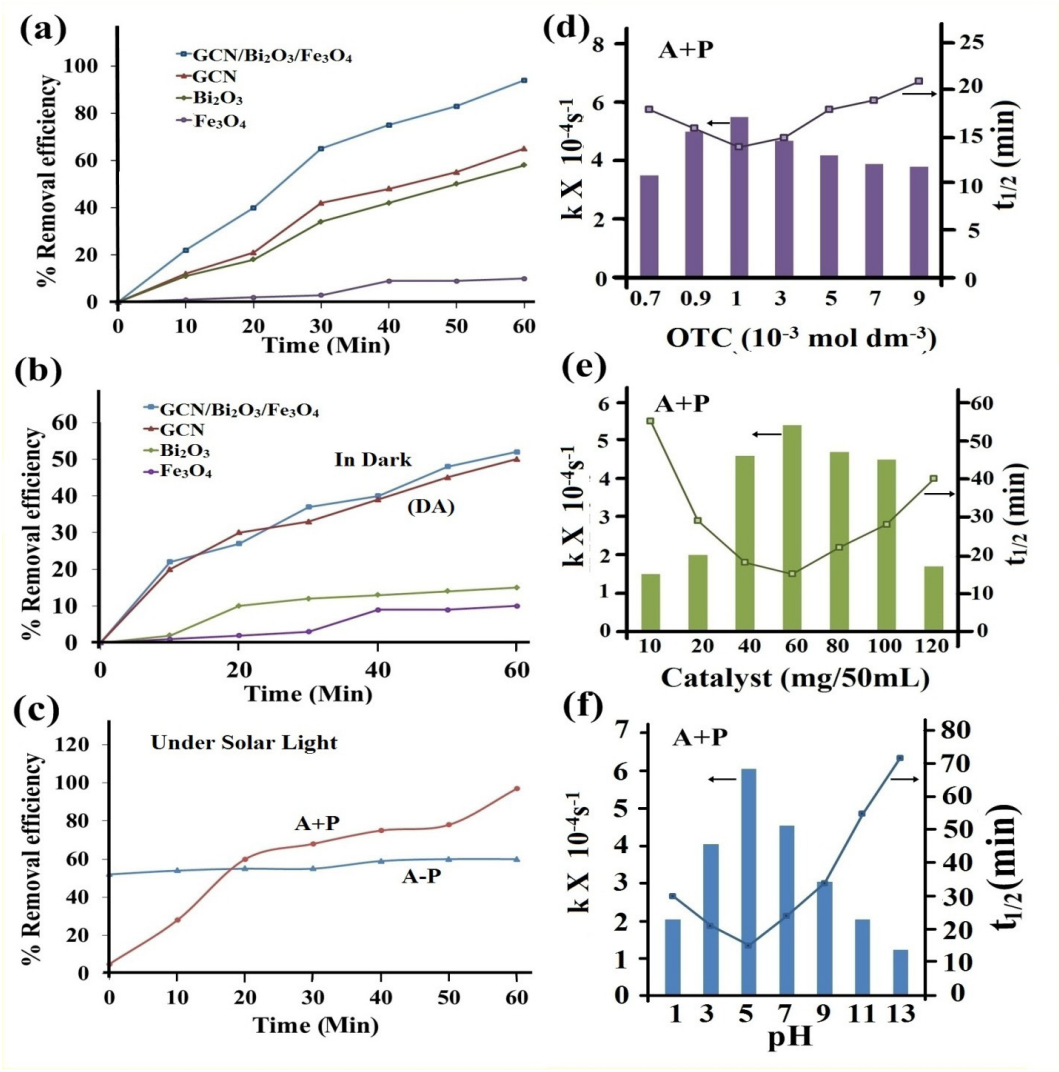

Fig. 8. (a) OTC degradation by different photocatalysts, (b) Adsorption in dark and (c) Photodegradation process under different reaction conditions, (d–f) Effect of reaction parameters on OTC degradation under solar system, (c) Effect of OTC concentration; (e) Effect of catalyst loading. (f) Effect of *p*H; Reaction conditions: [OTC] = 1 × 10^{-4} mol dm^{-3}; [catalyst] = 50 mg/100 ml ; pH = 5 .0; Solar light intensity = 35 × 10^3 ± 1000 lx; reaction time = 10 h.

The initial reaction pH solution plays an important role in photodegradation process. In present work reaction pH was varied from 1–13 to optimize reaction pH for OTC degradation and observed that rate constant increased from 2×10^{-4} s^{-1} to 6×10^{-4} s^{-1}due to pH increase from 1 to 5. However, rate constant was found to increase with increase in pH from 5 to 13. Above pHzpc and below pHzpc photocatalyst surface was primarily negatively charged but preeminence in catalyst surface was due to positively charged species. below pHzpc photocatalyst surface is positively charged (in acidic medium) whereas above pHzpc photocatalyst surface is negatively charged (in basic medium). In current research work, pHzpc of GCN/Bi_2O_3/Fe_3O_4 nanocomposite was examined to be 7.8. At low *p*H, both absorbent and OTC (antibiotic) were found to be positively charged as well as adsorption of OTC was lesser but with the increase in *p*H from acidic to basic, complete change in ionic species from positive charge to negative was observed for OTC [52]. OTC particles existed concurrent adsorption with photocatalysis in zwitter ionic form ($H_2OTC^{\pm}$) at pH 5 and OTC particles adsorption was higher whereas, OTC was found as $HOTC^-$ at pH 8.5 and $HOTC^{2-}$ at pH 11 [53]. Thus, at pH 5, these factors were main responsible reason for utmost photocatalytic eradication of OTC from simultaneous photocatalysis and adsorption from wastewater.

3.4. OTC (antibiotic) photocatalytic mineralization using GCN/Bi_2O_3/Fe_3O_4/A+P and GCN/Bi_2O_3/Fe_3O_4/A-P catalytic system

It was inferred from overhead discussion, that adsorption of OTC antibiotic on catalyst surface influenced photocatalytic activity of GCN/Bi_2O_3/Fe_3O_4/A+P as well as GCN/Bi_2O_3/Fe_3O_4/A+P photocatalytic systems. OTC photodegradation was studied for 10 h with A+P and A-P processes under solar light to attain thorough mineralization of antibiotic. The mineralization investigations were interpreted through

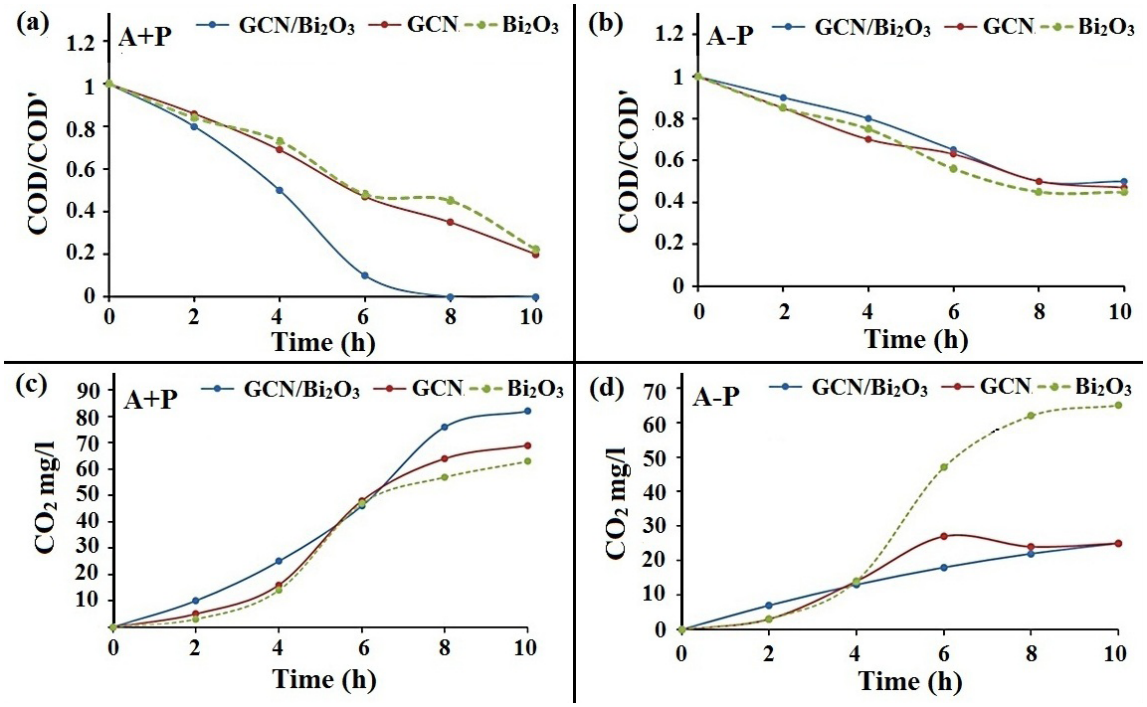

Fig. 9. Mineralization of OTC under solar light using A+P and A-P processes, a and d are COD removal graph. b and d are CO_2 evolution graph. Reaction conditions: [OTC] = 1×10^{-4} mol dm^{-3} ; [OTC]= 1×10^{-4} mol dm^{-3}; [catalyst] = 50 mg/100 ml ; pH = 5.0; Solar light intensity = $35 \times 10^3 \pm 1000$ lx; reaction time = 10 h.

COD and CO_2 removal during photocatalytic reaction (Figs. 9a–d).In case of A+P, 100, COD deduction attained was 65 and 55% for GCN/Bi_2O_3/Fe_3O_4, Bi_2O_3 and GCN, respectively [54]. During (A-P) process, GCN/Bi_2O_3/Fe_3O_4, GCN and Bi_2O_3 possessed respective 50, 53, 52% of COD removal for OTC degradation. During CO_2 evolution experiment, similar trend was observed for OTC mineralization process and CO_2 discharge detected during antibiotic degradation was also a sign of OTC mineralization. From above investigation, GCN/Bi_2O_3/Fe_3O_4/A+P emerged as most efficient catalytic system and it mineralized OTC completely in 8 h.

Furthermore, to explore mechanism of degradation process, trapping experiments were also applied using different scavengers for generated radicals such as isopropyl alcohol for $OH^{\bullet}$ radical, benzoquinone (BZQ) for O_2^{-}, ammonium oxalate (AO) for hole scavenger and Cr(VI) for electron [55]. With the addition of isopropyl alcohol, BZQ, ammonium oxalate and Cr(VI), the removal efficiency of OTC was 9, 36, 95 and 94%, respectively in 60 min (Fig. S2.). The addition of IPA and BZQ hindered removal efficiency of GCN/Bi_2O_3/Fe_3O_4 sharply, which indicated that $OH^{\bullet}$ and O_2^{-} radicals are mainly responsible for OTC degradation. The IPA is mainly used to understand degradation mechanism governed by $OH^{\bullet}$ radical due to its poor fixation with catalyst surface and rapid oxidation under aqueous medium [56].Furthermore, addition of AO and Cr(VI) scavengers had no substantial effect on OTC degradation and indicated that photogenerated h^{+}_{VB} and e^{-}_{CB} were not major reactive species during OTC removal. The decrease in photodegradation efficiency followed the trend: IPA > BZQ >> AQ > Cr(VI).

Fig. 8 illustrates photocatalytic activity of GCN/Bi_2O_3/Fe_3O_4 nanocomposites under solar light *via* proposed mechanism and on the basis of structure characterizations result and visible light photocatalytic tests of the prepared samples [57,58]. The calculated optical gap of are GCN and Bi_2O_3 are 2.7 and 2.8 eV, respectively. With respect to redox potential scale, the valence band (VB) edges of GCN and Bi_2O_3 were 1.4 eV and 3.13 eV and conduction band (CB) edges were –1.3 eV and 0.33 eV respectively (Fig. 10) [59,60]. The VB edge of GCN is more positive than Bi_2O_3, while CB edge of GCN is more negative than that of Bi_2O_3. In the presence of solar light, both GCN and Bi_2O_3 were able to produce charge carriers i.e. conduction band electrons (e^{-}_{CB}) and valence band holes (h^{+}_{VB}). The photogenerated h^{+}_{VB} in valence band of Bi_2O_3 shifted to valence band of GCN, whereas, CB electrons (e^{-}_{CB}) of GCN were migrated to CB of Bi_2O_3. Photo-oxidation and adsorption took place on or near photoactive surface. At *p*H ≈ 5, $HOTC^{-}$ was excited to singlet state and crossed triplet state of $HOTC^{-*}$ by intersystem crossing mechanism [61]. The triplet state $HOTC^{-*}$ returned to ground sate by donating electron to conduction band of Bi_2O_3 to generate superoxide anion radical (O_2^{-}). Thus, photo-induced electrons on the CB of GCN surface were easily transferred to Bi_2O_3 via interfaces and on the other hand holes on the Bi_2O_3 surface were migrated to GCN in a similar manner [33]. The charge transfer successfully retarded photogenerated electron hole pair recombination within two semiconducting materials causing an improvement in photocatalytic process. Electrons in conduction band combined with O_2 to produce O_2^{-} radicals and holes in valance band reacted with H^{+}/H_2O to generate hydroxyl radicals [62]. Thus, hydroxyl radicals and superoxide anion radicals ultimately mineralize OTC (pollutant) into CO_2, H_2O and respective ions.

3.5. Recyclability of GCN/Bi_2O_3/Fe_3O_4

Recycle efficiency is an important factor for large scale application of photocatalytic water treatment processes. The recycle efficiency of GCN/Bi_2O_3/Fe_3O_4 was explored for ten consecutive cycles under solar light. Photocatalyst separation from solution was accomplished using a permanent magnet for 90 s throughout each run,whereas, both GCN and Bi_2O_3 were separated in 20 min and 3 h using centrifugation and sedimentation process, respectively. The separated photocatalyst was washed thoroughly and dried for further use. The efficacy of GCN/Bi_2O_3/Fe_3O_4 was reduced to 90% from 99% for six consecutive cycles. However, in the case of GCN, efficacy was decreased to 57% from 65%. After ten cycles, recycle efficiency of Bi_2O_3 had a value of 48%. These findings indicated that magnetic GCN/Bi_2O_3/Fe_3O_4 possessed both higher recyclability and quicker separation from reaction solution (Fig. 11). However, the separation of GCN and Bi_2O_3 from reaction solution was slow and time consuming process. The present study revealed applicability of GCN/Bi_2O_3/Fe_3O_4 as a magnetic photocatalyst for wastewater remediation.

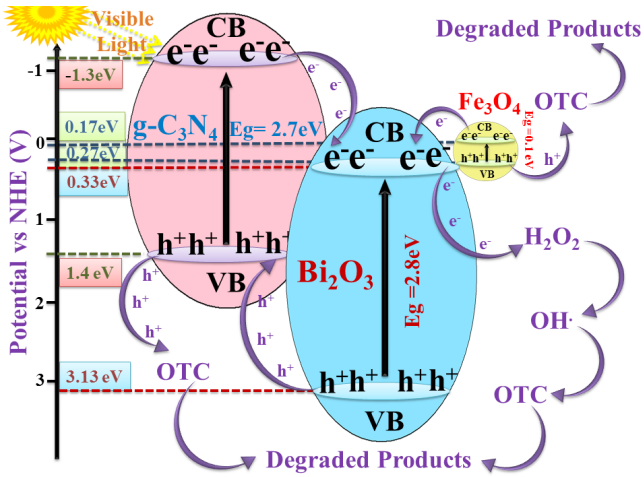

Fig. 10. Proposed mechanism for OTC degradation using GCN/Bi_2O_3/Fe_3O_4 photocatalyst.

4. Conclusion

Finally, it was concluded that highly efficient and reusable GCN/Bi_2O_3/Fe_3O_4 composites were synthesized by simple hydrothermal method. SEM, TEM, XRD, FTIR and EDX different analyses techniques were executed to confirm the formation of GCN/Bi_2O_3/Fe_3O_4 nanocomposites. The synthesized GCN/Bi_2O_3/Fe_3O_4 nanocomposite was separated from reaction solution in 90 s through a magnet. GCN/Bi_2O_3/

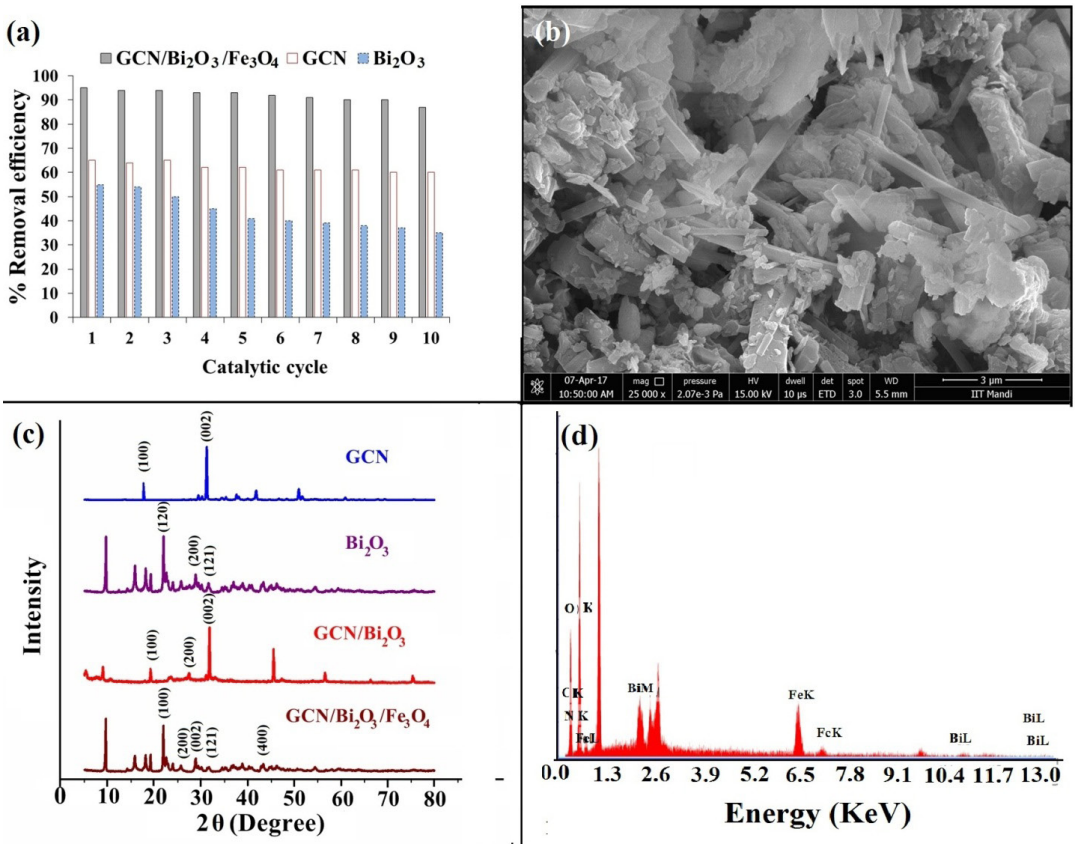

Fig. 11. Recycle efficiency of photocatalysts. [OTC] = 1 × 10^{-4} mol dm^{-3}; [OTC] = 1 × 10^{-4} mol dm^{-3}; [catalyst] = 50 mg/100 ml ; pH = 5.0; Solar light intensity = 35 × 10^3± 1000 lx; reaction time = 10 h.

Fe_3O_4 nanocomposite possessed photocatalytic activity for antibiotic (OTC) degradation and revealed significant adsorption capacity for antibiotic (OTC) eradication from water. A+P (concurrent adsorption with photocatalysis) process exhibited synergistic effect for OTC degradation and within 8 h mineralization was obtained. The degradation process mainly occurred by hydroxyl radical formation mechanism. Substantial recycle efficacy was perceived by magnetically separated photocatalysts for 10 catalytic cycles. The GCN/Bi_2O_3/Fe_3O_4 ternary nanocomposite also proposed a new outlook to develop novel and efficient photocatalytic materials for industrial and pharmaceutical waste water treatment.

References

[1] J.M. Brausch, G.M., Rand, A review of personal care products in the aquatic environment: environmental concentrations and toxicity, Chemosphere, 82 (2011) 1518–1532.

[2] A Sudhaik, P. Raizada, P. Shandilya, P. Singh, Magnetically recoverable graphitic carbon nitride and $NiFe_2O_4$ based magnetic photocatalyst for degradation of oxytetracycline antibiotic in simulated wastewater under solar light, J. Environ. Chem. Eng., 6(4) (2018) 3874–3883.

[3] P. Shandilya, D. Mittal, M. Soni, P. Raizada, A. Hosseini-Bandegharaei, A.K. Saini, P. Singh, Fabrication of fluorine doped graphene and $SmVO_4$ based dispersed and adsorptive photocatalyst for abatement of phenolic compounds from water and bacterial disinfection, J. Cleaner Prod., 203 (2018) 386-399.

[4] P. Shandilya, D. Mittal, A. Sudhaik, M. Soni, P. Raizada, A. K. Saini, P. Singh, $GdVO_4$ modified fluorine doped graphene nanosheets as dispersed photocatalyst for mitigation of phenolic compounds in aqueous environment and bacterial disinfection, Sep. Purif. Technol., 210 (2019) 804–816.

[5] S. Gautam, P. Shandilya, B. Priya, V.P. Singh, P. Raizada, R. Rai, M.A. Valente, P. Singh, Superparamagnetic $MnFe_2O_4$ dispersed over graphitic carbon sand composite and bentonite as magnetically recoverable photocatalyst for antibiotic mineralization, Sep. Purif. Technol., 172 (2017) 498–511.

[6] P. Shandilya, D. Mittal, M. Soni, P. Raizada, J.H. Lim, D.Y. Jeong, R.P. Dewedi, A.K. Saini, P. Singh, Islanding of $EuVO_4$ on high-dispersed fluorine doped few layered graphene sheets for efficient photocatalytic mineralization of phenolic compounds and bacterial disinfection, J. Taiwan Inst. Chem. Eng., 93 (2018) 528–542.

[7] B. Priya, P. Shandilya, P. Raizada, P. Thakur, N. Singh, P. Singh, Photocatalytic mineralization and degradation kinetics of ampicillin and oxytetracycline antibiotics using graphene sand composite and chitosan supported BiOCl, J. Mol. Catal. A: Chemical, 423 (2016) 400–413.

[8] B. Pare, P. Singh, S.B. Jonnalgadda, Artificial light assisted photocatalytic degradation of lissamine fast yellow dye in ZnO suspension in a slurry batch reactor, Indian J. Chem., 48 (2009) 1364–1369.

[9] C. Ye, J.X. Li, Z.J. Li, X.B. Li, X.B. Fan, L.P. Zhang, B. Chen, C.H. Tung, L.Z. Wu, Enhanced driving force and charge separation efficiency of protonated g-C_3N_4 for photocatalytic O_2 evolution, ACS Catal., 5 (2015) 6973–6979.

[10] Y. Huan, D. Huang, G. Zeng, C. Lai, L. Qin, M. Cheng, S. Ye, B. Song, X. Ren, X. Guo, Selective prepared carbon nanomaterials for advanced photocatalytic application in environmental pollutant treatment and hydrogen production, Appl. Catal. B: Environ., (2018).

[11] K. Maeda, K. Teramura, D.L. Lu, T. Takata, N. Saito, Y. Inoue, K. Domen, Photocatalyst releasing hydrogen from water, Nature, 440 (2006) 295.

[12] A. Sudhaik, P. Raizada, P. Shandilya, D.Y. Jeong, J.H. Lim, P. Singh, Review on fabrication of graphitic carbon nitride based efficient nanocomposites for photodegradation of aqueous phase organic pollutants, J. Ind. Eng. Chem., 67 (2018) 28–51.

[13] P. Raizada, A. Sudhaik, P. Singh, P. Shandilya, P. Thakur, H. Jung, Visible light assisted photodegradation of 2, 4-dinitrophenol using Ag_2CO_3 loaded phosphorus and sulphur co-doped graphitic carbon nitride nanosheets in simulated wastewater, Arab. J. Chem. (2018).

[14] Y. Huan, G. Zeng, C. Lai, D. Huang, L. Tang, J. Gong, M. Chen, P. Xu, H. Wang, M. Cheng, C. Zhang, W. Xiong, Environment-friendly fullerene separation methods, Chem. Eng. J., 330 (2017) 134–145.

[15] Z. Zhao, Y. Sun, F. Dong, Graphitic carbon nitride based nanocomposites: a review, Nanoscale, 7 (2015) 15–37.

[16] M.N. Gómez-Cerezo, M.J. MunMarcos, D. Tudela, M. Fernández-Garcíaa, A. Kubackaa, Composite Bi_2O_3–TiO_2 catalysts for toluene photo-degradation: ultraviolet and visible light performances, Appl. Catal. B, 156–157 (2014) 307–313.

[17] W.T. Dong, C.S. Zhu, Optical properties of surface-modified Bi_2O_3 nanoparticles, J. Phys. Chem. Solids, 64 (2003) 265–271.

[18] M. Xiong, L. Chen, Q. Yuan, J. He, S.L. Luo, C.T. Au, S.F. Yin, Controlled synthesis of graphitic carbon nitride/beta bismuth oxide composite and its high visible-light photocatalytic activity, Carbon, 86 (2015) 217–224.

[19] Y.N. Huo, X.F. Chen, J. Zhang, G.F. Pan, J.P. Jia, H.X. Li, Ordered macroporous Bi_2O_3/TiO_2 film coated on a rotating disk with enhanced photocatalytic activity under visible irradiation, Appl. Catal. B, 148–149 (2014) 550–556.

[20] B. Priya, P. Raizada, N. Singh, P. Thakur, P. Singh, Adsorptional photocatalytic mineralization of oxytetracycline and ampicillin antibiotics using $B_{i2}O_3$/BiOCl supported on graphene sand composite and chitosan, J. Colloid. Inter. Sci., 47 (2016) 271–283.

[21] K.T. Ranjit, B. Viswanthan, Synthesis, characterization and photocatalytic properties of iron-doped TiO_2 catalysts, J. Photochem. Photobiol. A, 108 (1997) 79–84.

[22] S. Gautam, P. Shandilyaa, V.P. Singh, P. Raizada, P. Singh, Solar photocatalytic mineralization of antibiotics using magnetically separable $NiFe_2O_4$ supported onto graphene sand composite and bentonite, J. Water Process. Eng., 14 (2016) 86–100.

[23] W.L. Kostedt, J. Drwiega, D.W. Mazyck, S.W. Lee, W. Sigmund, C.Y. Wu, P. Chadik, Magnetically agitated photocatalytic reactor for photocatalytic oxidation of aqueous phase organic pollutants, Environ. Sci. Technol., 39 (2005) 8052–8056.

[24] S. Gautam, P. Shandilya, B. Priya, V.P. Singh, P. Raizada, P. Singh, Graphene bentonite supported $ZnFe_2O_4$ as superparamagnetic photocatalyst for antibiotic degradation, Adv. Mater. Lett., 8(3) (2017) 229–238.

[25] J. Navio, G. Colon, M. Trillas, J. Peral, X. Domenech, J.J. Testa, J. Padron, D. Rodriguez, M.I. Litter, Heterogeneous photocatalytic reactions of nitrite oxidation and Cr(VI) reduction on iron-doped titania prepared by the wet impregnation method, Appl. Catal. B, 16 (1998) 187–196.

[26] K.T. Ranjit, B. Viswanthan, Synthesis, characterization and photocatalytic properties of iron-doped TiO_2 catalysts, J. Photochem. Photobiol. A, 108 (1997) 79–84.

[27] M.I. Litter, J.A. Navio, Comparison of the photocatalytic efficiency of TiO_2, iron oxides and mixed Ti (IV)-Fe (III) oxides: photodegradation of oligocarboxylic acids, J. Photochem. Photobiol. A, 84 (1994) 183–193.

[28] Z.Y. Lu, X.X. Zhao, Z. Zhu, Y.S. Yan, W.D. Shi, H.J. Dong, Z.F. Ma, N.L. Gao, Y.S. Wang, H. Huang, Enhanced recyclability, stability, and selectivity of CdS/C@Fe_3O_4 nanoreactors for orientation photodegradation of ciprofloxacin, Chem. Eur. J., 21 (2015) 18528–18533.

[29] X.F. Bian, K.Q. Hong, L.Q. Liu, M.X. Xu, Magnetically separable hybrid CdS-TiO_2-Fe_3O_4 nanomaterial: Enhanced photocatalytic activity under UV and visible irradiation, Appl. Surf. Sci., 280 (2013) 349–353.

[30] W. Wu, C.Z. Jiang, V.A.L. Roy, Recent progress in magnetic iron oxide–semiconductor composite nanomaterials as promising photocatalysts, Nanoscale, 7 (2015) 38–58.

[31] P. Singh, Sonu, P. Raizada, A. Sudhaik, P. Shandilya, P. Thakur, S. Agarwal, V.K. Gupta, Enhanced photocatalytic activity and stability of AgBr/BiOBr/graphene heterojunction for phenol degradation under visible light, J. Saudi Chem. Soc., (2018).

[32] J. Xian, D. Li, J. Chen, X. Li, M. He, Y. Shao, L. Yu, J. Fang, TiO_2 Nanotube array graphene/CdS quantum dots composite film in Z-scheme with enhanced photoactivity and photostability, ACS Appl. Mater. Interfaces, 6 (2014) 13157–13166.
[33] Y. Li, S. Wu, L. Huang, H. Xu, R. Zhang, M. Qu, Q. Gao, H. Li, g-C_3N_4 modified Bi_2O_3 composites with enhanced visible-light photocatalytic activity, J. Phys. Chem. Solid., 76 (2015) 112–119.
[34] Y. Zhang, J. Lu, M.R. Hoffmann, Q. Wang, Y. Conga, Q. Wang, H. Jin, Synthesis of g-C_3N_4/Bi_2O_3/TiO_2 composite nanotubes: enhanced activity under visible light irradiation and improved photoelectrochemical activity, RSC Adv., 5 (2015) 48983–48991.
[35] L. Huang, H. Xu, Y. Li, H. Li, X. Cheng, J. Xia, Y. Xu, G. Cai, Visible-light-induced WO_3/g-C_3N_4 composites with enhanced photocatalytic activity, Dalton Trans., 42 (2013) 8606–8616.
[36] T. Tyborski, C. Merschjann, S. Orthmann, F. Yang, M.C. Lux-Steiner, T. Schedel-Niedrig, Tunable optical transition in polymeric carbon nitrides synthesized via bulk thermal condensation, J. Phys.: Condens. Matter., 24 (2012) 162201.
[37] J. Zhang, Y. Li, P. Zhu, D. Huang, S. Wu, Q. Cui, G. Zou, Graphitic carbon nitride materials synthesized via reactive pyrolysis routes and their properties, Diam. Relat. Mater., 20 (2011) 385–388.
[38] L. Liu, J. Jiang, S. Jin, Z. Xia, M. Tang, Hydrothermal synthesis of β-bismuth oxide nanowires from particles, Cryst. Eng. Comm., 13 (2011) 2529–2532.
[39] A.F. Gualtieri, S. Immovilli, M. Prudenziati, Powder X-ray diffraction data for the new polymorphic compound ω-Bi_2O_3, Powder Diffr., 12 (1997) 90–92.
[40] S. Kumar, T. Surendar, B. Kumar, A. Baruah, V. Shanker, Synthesis of magnetically separable and recyclable g-C_3N_4–Fe_3O_4 hybrid nanocomposites with enhanced photocatalytic performance under visible-light irradiation, J. Phys. Chem. C, 117(49) (2013) 26135–26143.
[41] Q. Zhuang, L. Sun, Y. Ni, One-step synthesis of graphitic carbon nitride nanosheets with the help of melamine and its application for fluorescence detection of mercuric ions, Talanta, 164 (2017) 458–462.
[42] R. Irmawati, M.N.N. Nasriah, Y.H. Taufig-Yap, S.B.A. Hamid, Characterization of bismuth oxide catalysts prepared from bismuth trinitrate pentahydrate: influence of bismuth concentration, Catal. Today, 93–95 (2004) 701–709.
[43] Y.J. Cui, Z.X. Ding, X.Z. Fu, X.C. Wang, Construction of conjugated carbon nitride nanoarchitectures in solution at low temperatures for photoredox catalysis, Angew. Chem., 124(47) (2012) 11984–11988.
[44] H.J. Cui, J.W. Shi, B. Yuan, M.L. Fu, Synthesis of porous magnetic ferrite nanowires containing Mn and their application in water treatment, J. Mater. Chem. A, 1 (2013) 5902–5907.
[45] H.Y. Zhu, R. Jiang, S.H. Huang, J. Yao, F.Q. Fu, J.B. Li, Novel magnetic $NiFe_2O_4$/multi-walled carbon nanotubes hybrids: facile synthesis, characterization, and application to the treatment of dyeing wastewater, Ceram. Int., 41 (2015) 11625–11631.
[46] M. Yu, J. Lin, J. Fang, Silica Spheres Coated with YVO_4: Eu^{3+} Layers via sol-gel process: a simple method to obtain spherical core- shell phosphors, Chem. Mater., 17 (2005) 1783–1791.
[47] L. Xiong, W. Sun, Y. Yang, C. Chen, J. Ni, Heterogeneous photocatalysis of methylene blue over titanate nanotubes: Effect of adsorption, J. Colloid. Interf. Sci., 356 (2011) 211–216.
[48] B. Pare, P. Singh, S.B. Jonnalagadda, Visible light-driven photocatalytic degradation and mineralization of neutral red dye in a slurry photoreactor, Ind. J. Chem. Technol., 17 (2010) 391.
[49] P. Raizada, J. Kumari, P. Shandilya, R. Dhiman, V.P. Singh, P. Singh, Magnetically retrievable Bi_2WO_6/Fe_3O_4 immobilized on graphene sand composite for investigation of photocatalytic mineralization of oxytetracycline and ampicillin, Process Saf. Environ. Prot., 106 (2017) 104–116.
[50] P. Raizada P. Singh, A. Kumar, G. Sharma, D. Pathania, P. Thakur, Solar photocatalytic activity of nano-ZnO supported on activated carbon or brick grain particles: role of adsorption in dye degradation, Appl. Catal. A, 486 (2014) 159–169.
[51] B. Gao, T.M. Lim, D.P. Subagio, T.T. Lim, Zr-doped TiO_2 for enhanced photocatalytic degradation of bisphenol A, Appl. Catal. A, 375 (2010) 107–115.
[52] P. Raizada, S. Gautam, B. Priya, P. Singh, Preparation and photocatalytic activity of hydroxyapatite supported BiOCl nanocomposite for oxytetracyline removal, Adv. Mater. Lett., 7(4) (2016) 312–318.
[53] S.K. Kansal, M. Singh, D. Sud, Studies on photodegradation of two commercial dyes in aqueous phase using different photocatalysts, J. Hazard. Mater., 141 (2007) 581–590.
[54] P. Singh, P. Raizada, A. Kumar, P. Thakur, Preparation of BSA-$ZnWO_4$ nanocomposites with enhanced adsorptional photocatalytic, Int. J. Photoenergy, 7 (2013) 7.
[55] V. Buxton. C. Greenstock, W.P. Hellman, A.P. Ross, Critical review of rate constants for reactions of hydrated electrons, hydrogen atoms and hydroxyl radicals (·OH/·O^- in aqueous solution, J. Phys. Chem. Ref Data, 17 (1988) 513–886.
[56] B. Priya, P. Shandilya, P. Raizada, P. Thakur, N. Singh, P. Singh, Photocatalytic mineralization and degradation kinetics of ampicillin and oxytetracycline antibiotics using graphene sand composite and chitosan supported BiOCl, J. Mol. Catal. A: Chemical, 423 (2016) 400–413.
[57] P. Raizada, P. Shandilya, P. Singh, P. Thakur, Solar light-facilitated oxytetracycline removal from the aqueous phase utilizing a H_2O_2/$ZnWO_4$/CaO catalytic system, J. Taibah Uni. Sci., 11 (2017) 689–699.
[58] P. Xu, G.M. Zeng, D.L. Huang, C.L. Feng, S. Hu, M.H. Zhao, C. Lai, Z. Wei, C. Huang, G.X. Xie, Z.F. Liu, Use of iron oxide nanomaterials in wastewater treatment: a review, Sci. Total Environ., 424 (2012) 1–10.
[59] H.M. Fan, H.Y. Li, B.K. Liu, Y.C. Lu, T.F. Xie, D.J. Wang, Photoinduced charge transfer properties and photocatalytic activity in Bi_2O_3/$BaTiO_3$ composite photocatalyst, ACS Appl. Mater. Interfaces, 4 (2012) 4853–4857.
[60] S.C. Yan, S.B. Lv, Z.S. Li, Z.G. Zou, Organic–inorganic composite photocatalyst of g-C_3N_4 and TaON with improved visible light photocatalytic activities, Dalton Trans., 39 (2010) 1488–1491.
[61] C. Zhao, M. Pelaez, X. Duan, D.D. Dionysiou, Role of pH on photolytic and photocatalytic degradation of antibiotic oxytetracycline in aqueous solution under visible/solar light: kinetics and mechanism studies, Appl. Catal. B, 134 (2013) 83–92.
[62] J.L. Hu, H.M. Li, C.J. Huang, M. Liu, X.Q. Qiu, Enhanced photocatalytic activity of Bi_2O_3 under visible light irradiation by Cu(II) clusters modification, Appl. Catal. B: Environ., 142–143 (2013) 598–603.

Supplementary

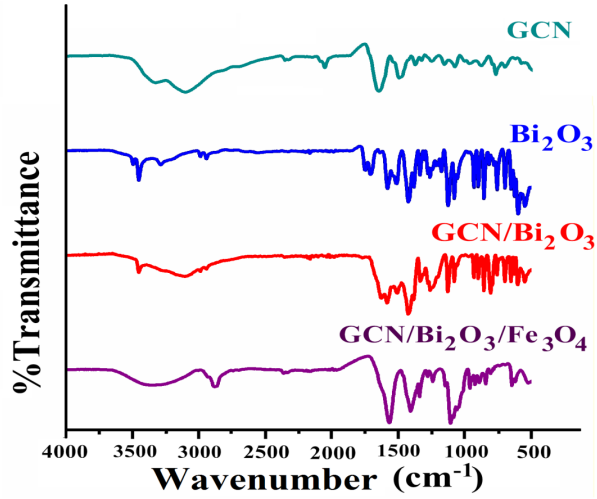

Fig. S1. FTIR spectra of GCN, Bi_2O_3, GCN/Bi_2O_3 and GCN/Bi_2O_3/Fe_3O_4.

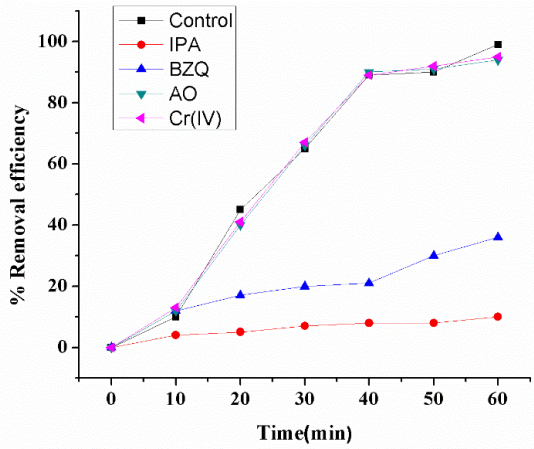

Fig. S2. Effect of radical scavengers on photocatalytic degradation of OTC. [OTC] = 1 × 10^{-4} mol dm^{-3}; [Scavenger] = [1 × 10^{-6} mol dm^{-3}]; [catalyst] = 50 mg/100 ml ; pH = 5 .0; Solar light intensity = 35 × 10^3 ± 1000 lx;